Theoretical and Experimental Comparison of Indirect Field-Oriented Controllers for Induction Motors

Sergei Peresada, Andrea Tilli, and Alberto Tonielli, *Associate Member, IEEE*

***Abstract*—A theoretical and experimental comparison between standard and recently-developed improved indirect field-oriented controllers for induction motors is presented. It is shown that standard indirect field-oriented control algorithm provides asymptotic speed and flux regulation, while the improved one guarantees global exponential speed–flux tracking under condition of constant load torque. The difference between the flux sub-system design for the two controllers is analyzed. It is shown that the improved controller provides closed loop properties for flux subsystem when motor is rotating, leading to robust stabilization of the rotor flux vector space position and robust tracking of its modulus. It is demonstrated that both controllers have similar complexity and can be tuned using standard procedure for cascaded systems. Intensive experimental study shows that improved controller provides about one order higher speed tracking performance as compared with standard solution. Moreover, improved robustness with respect to rotor parameters variation leads to improved energy efficiency and robust stabilization of dynamic performance.**

***Index Terms*—Energy efficiency, electric drives, nonlinear control, vector control.**

NOMENCLATURE

ω	Rotor speed.
ω_0, ε_0	Speed and angular position of the (d–q) reference frame.
T_L	Load torque.
J	Total inertia.
$\mathbf{i} = (i_d, i_q)^T$	Stator current vector represented in (d–q) reference frame.
$\mathbf{u} = (u_d, u_q)^T$	Stator voltage vector represented in (d–q) reference frame.
$\boldsymbol{\psi} = (\psi_d, \psi_q)^T$	Rotor flux vector represented in (d–q) reference frame.
$\mathbf{z}^*$	Reference value for vector $\mathbf{z}$.
$\hat{T}_L$	Estimate of $T_L/J = \text{const}$..
$\tilde{T}_L = T_L/J - \hat{T}_L$	Estimation error.
$\tilde{\mathbf{z}} = \mathbf{z} - \mathbf{z}^*$	Vector of regulation errors.
R_s, R_r, L_s, L_r	Stator/rotor resistances and inductances.
L_m	Magnetizing inductance.
σ, β, μ, α, γ	Positive constants related to electrical and mechanical parameters of IM.
k_{xx}, λ	Tuning gains of the controllers.

Manuscript received January 4, 2002; revised October 1, 2002. This work was supported by Project MIUR-PRSIN-20011093788_004 "Innovative Methodologies and Tools for the Design of Mechatronic Systems." Recommended by Associate Editor J. Ojo.

S. Peresada is with the Department of Electrical Engineering, National Technical University of Ukraine, Kiev Polytechnic Institute, Kiev 252056, Ukraine (e-mail: peresada@i.com.ua).

A. Tilli and A. Tonielli are with the Department of Electronics, Computer and System Sciences (DEIS), University of Bologna, Bologna 40136, Italy (e-mail: atilli@deis.unibo.it; atonielli@deis.unibo.it).

Digital Object Identifier 10.1109/TPEL.2002.807123

I. INTRODUCTION

VECTOR controlled induction motor (IM) drives are wide spread electromechanical systems suitable for high dynamic performance applications. The concept of field orientation [1], as a torque–flux decoupling technique applied to IM control [2], [3], was the background for the development of commercial vector controlled IM drives, quite before the modern theory of nonlinear feedback control was applied for control of electric machines.

Control algorithms based on direct field orientation (DFO) use a flux observer, hence nonlinear flux observers have been widely developed [4]–[6]. Control algorithms based on indirect field orientation (IFO) use the reference values for flux vector (modulus and angle) instead of the estimated one. The idea of indirect field orientation has been considered first in [7].

Although their properties were not strongly theoretically proven, both DFO and IFO solutions have been implemented in industrial drives demonstrating performances suitable for a wide spectrum of technological applications. This stimulated a significant research activity to develop IM vector control algorithms using nonlinear control theory in order to improve performances, achieving speed (or torque) and flux tracking, or to give a theoretical justification of the existing solutions. In fact, the first proof of exponential asymptotic stability for Standard IFO (S-IFO) control, adopted in industrial drives, is given only in [8] under the following assumptions: current-fed IM (reduced-order solution); known IM parameters; constant speed and flux references. It is shown that S-IFO controller can be derived using passivity theory [9]. In [10] a full order IFO-controller, which solves the problem of global asymptotic speed and rotor flux modulus tracking in presence of unknown constant load torque is developed. Nevertheless, algorithm reported in [10] is more complex than S-IFO and requires to tune a larger number of control gains.

Since in solutions based on concept of IFO the flux control is open loop, the flux subsystem is sensitive to IM rotor parameters variation, especially the rotor resistance (see [11] and references included). As a consequence of parameter perturbations the field orientation is missed, leading to errors in rotor flux vector control (modulus and angle). The wrong field orientation causes degradation of speed transient performance and reduced IM energy efficiency.

0885-8993/03$17.00 © 2003 IEEE

The parameter sensitivity problem of a standard IM vector control algorithms is well stated and several solutions have been considered to improve the flux vector control accuracy [5], [6], [11]–[14]. Regarding flux estimation [5], [6] for DFO solutions, it is proposed to use so-called "voltage model" during operation at high speeds and "current model" for low speeds. Different modifications are possible using full order flux observers [4], [12], which include both IM stator and rotor circuit models. An alternative approach is based on adaptive system theory and it has been applied to DFO [13], [11] and IFO schemes (see [14] and reference included). Being observerless solutions, IFO controllers have less degrees of freedom in control design in order to improve robustness. As result, robust IFO control for IM is still far from a definite solution. Some promising ideas of application of the artificial intelligence approaches to basic field oriented vector controllers of IM are reported in [15], including speed sensorless control, which is the main recent trend in IM control.

Recently, in [16] the authors proposed a new Improved Indirect Field-Oriented (I-IFO) control algorithm, which can be viewed as a step in solving the problem of robust indirect field oriented control of IM. Specifically, the problem of flux–speed tracking has been addressed in the presence of unknown constant load torque and under the requirement of achieving new features for the closed loop dynamics such as: global exponential asymptotic speed–flux tracking; asymptotic speed–flux decoupling; asymptotic linearization of the speed subsystem; robustness with respect to IM parameter (especially rotor resistance) variations. Note that proof of the exponential stability is one of the important points for robustness analysis via general stability arguments.

The above-reported analysis has been focused on the speed–flux control algorithms proposed in literature whose properties (at least stability) have been analytically proven and experimentally validated. Some important issues related to the problem discussed can be also found in [17]. Only few results on experimental comparison study of different control algorithms have been reported in literature so far. Among them [11], where an adaptive and a nonadaptive observer-based control algorithm of current-fed IM have been compared; [14], where an adaptive and a nonadaptive indirect field-oriented controllers are investigated; [18], where the nonadaptive version of [11] is compared with the S-IFO controller for current-fed IM, and [10], where full order S-IFO controller and a full-order speed–flux tracking controller were experimentally tested. Some results on implementation of the S-IFO controller (passivity based, according to [9]) are also reported in [19].

The necessary condition for adequate comparison of different control algorithms is to assure that they are studied in comparable conditions. Another important methodological question for such comparison is how to define the control algorithm that can serve as a touchstone. From analysis of [10], [11], [14] and [18], it follows that the natural choice is the full-order S-IFO controller, whose dynamic behavior is well recognizable from available industrial products. Nevertheless, the stability and structural properties of the full-order S-IFO controllers have not been investigated yet.

The aim of this paper is to evaluate the dynamic performance and the robustness of the I-IFO, proposed in [16], by means of theoretical and experimental comparison with the S-IFO control algorithm. Both S-IFO and I-IFO controllers are based on the stator currents and speed measurements. First it is shown how the S-IFO control can be reinterpreted in terms of nonlinear control theory. It is proven that the full-order speed–flux error dynamics generated by S-IFO controllers is at least locally asymptotically stable, which ensures the practical asymptotic stability for typical IM operating conditions. From the analysis of the structural properties of the equivalent error dynamics generated by S-IFO and I-IFO solutions, it results that the two controllers are presented in a configuration which allows adequate comparison, providing the same tuning of proportional and integral gains of current and speed controllers. It is shown that the dynamics of the I-IFO controller presents a "nominal speed-error subsystem" which is linear and time-invariant for time-varying speed–flux references and has a regular structure, independent of electric machine parameters. Moreover, it is enlighten that the flux subsystem of the S-IFO controller is open loop with respect to flux errors, while the I-IFO flux controller provides *closed loop properties* of the flux error dynamics when the motor is rotating. The closed loop structure of the flux error dynamics guarantees the robust stabilization of the rotor flux vector also under rotor parameters variations.

The experimental tests of the two controllers carried-out include the investigation of the dynamic performance during speed trajectory tracking and step load torque rejection as well as evaluation of the efficiency of the electromechanical energy conversion process during steady state. Operating conditions with nominal parameters and with variation of the rotor time-constant have been considered.

The conclusions of the comparison can be summarized as follows:

1) both controllers require the same computational power for real time implementation;
2) the tuning procedure of control gains is conceptually the same for the two controllers;
3) the I-IFO speed–flux controller has speed tracking performance about one-order higher than the S-IFO controllers;
4) the I-IFO controller provides robust stabilization of the rotor flux vector (condition of field orientation).

In particular, the last results leads to two relevant properties under condition of varying rotor parameters: a) better energy efficiency (up to 30% in experimental test) of the I-IFO controller as compared with S-IFO one; b) robust invariance of the dynamic properties of I-IFO solution, while the S-IFO shows large degradation. It is experimentally proven that I-IFO control demonstrates robustness properties with respect to rotor time constant variation closed to that of adaptive controllers [11] and [14], if the rotor speed is not null.

The paper is organized as follows: in Section II the IM model and the control problem statements are given; Sections III and IV present theoretical and experimental comparison of the two controllers.

II. Induction Motor Model and Control Problem Statement

A. Induction Motor Model

Under the assumptions of linear magnetic circuits and balanced operating conditions the equivalent two-phase model of the symmetrical IM, represented in an arbitrary rotating reference frame (d–q), is

$$\begin{aligned}\dot{\omega} &= \mu(\psi_d i_q - \psi_q i_d) - \frac{1}{J} T_L \\ \dot{\boldsymbol{\psi}} &= -\alpha\boldsymbol{\psi} - (\omega_0 - \omega)\mathbf{J}\boldsymbol{\psi} + \alpha L_m \mathbf{i} \\ \dot{\mathbf{i}} &= -\gamma\mathbf{i} - \omega_0\mathbf{J}\mathbf{i} + \alpha\beta\boldsymbol{\psi} - \beta\omega\mathbf{J}\boldsymbol{\psi} + \frac{1}{\sigma}\mathbf{u} \end{aligned} \tag{1}$$

$$\dot{\varepsilon}_0 = \omega_0; \qquad \varepsilon_0(0) = 0 \tag{2}$$

where ω is the rotor speed, $\mathbf{i} = (i_d, i_q)^T$, $\boldsymbol{\psi} = (\psi_d, \psi_q)^T$ denote stator current and rotor flux vectors, $\mathbf{u} = (u_d, u_q)^T$ is the control voltage vector. Subscripts d and q stand for vector components in the (d–q) reference frame, T_L is the load torque, ε_0 is the angular position of the (d–q) reference frame with respect to the fixed stator reference frame (a–b), where the physical variables are defined. The transformed variables are given by

$$\begin{aligned}\mathbf{x}_{dq} &= \mathbf{e}^{-\mathbf{J}\varepsilon_0}\mathbf{x}_{ab} \\ \mathbf{x}_{ab} &= \mathbf{e}^{\mathbf{J}\varepsilon_0}\mathbf{x}_{dq}\end{aligned} \qquad \text{where } \mathbf{e}^{-\mathbf{J}\varepsilon_0} = \begin{bmatrix} \cos\varepsilon_0 & \sin\varepsilon_0 \\ -\sin\varepsilon_0 & \cos\varepsilon_0 \end{bmatrix},$$
$$\mathbf{J} = \begin{bmatrix} 0 & -1 \\ 1 & 0 \end{bmatrix} \tag{3}$$

where $\mathbf{x}_{yz}$ stands for two-dimensional voltage, flux and current vectors.

Positive constants related to the electrical and mechanical parameters of the IM are defined as

$$\sigma = L_s\left(1 - \frac{L_m^2}{L_s L_r}\right), \quad \beta = \frac{L_m}{\sigma L_r}, \quad \mu = \frac{3}{2}\frac{L_m}{JL_r},$$
$$\alpha = \frac{R_r}{L_r}, \quad \gamma = \left(\frac{R_s}{\sigma} + \alpha L_m \beta\right)$$

where J is the rotor inertia, R_s, R_r, L_s, L_r are stator/rotor resistances and inductances respectively, L_m is the magnetizing inductance. One pole pair is assumed without loss of generality.

B. IM Control Objectives Under Condition of Indirect Field Orientation

The concept of field orientation (FO) was developed by Blaschke [1] as a torque–flux decoupling technique applied to IM control (see [2]). Let briefly recall important properties related to the indirect formulation of this concept.

General specifications for speed-controlled electric drives indicate that two IM outputs, speed and rotor flux modulus, defined as

$$\mathbf{y}_1 = \begin{bmatrix} \omega \\ \sqrt{\psi_d^2 + \psi_q^2} \end{bmatrix} \triangleq \begin{bmatrix} \omega \\ |\psi| \end{bmatrix} \tag{4}$$

must be controlled using the two dimensional stator voltage vector $\mathbf{u}$ on the basis of measured variables vector $\mathbf{y} = (\omega, i_d, i_q)^T$. The load torque T_L is considered as an unknown constant (linearly parameterized) disturbance. In the case of indirect field-oriented control, the dynamics of the (d–q) reference frame (2) is specified in such a way that the d-axis of the reference frame is asymptotically aligned with the direction of the rotor flux vector, i.e.

$$\lim_{t\to\infty} \psi_d = |\psi|, \qquad \lim_{t\to\infty} \psi_q = 0. \tag{5}$$

Defining ω^*, $\psi^* > 0$ as the reference trajectories for speed and flux, the speed and flux-modulus tracking (regulation) errors can be written as

$$\begin{aligned}\tilde{\omega} &= \omega - \omega^* \\ \tilde{\psi}_d &= \psi_d - \psi^* \\ \tilde{\psi}_q &= \psi_q. \end{aligned} \tag{6}$$

According to condition of field orientation (5) and error definition (6) the IM control objective (4) is given by

$$\lim_{t\to\infty} \tilde{\omega} = 0, \quad \lim_{t\to\infty} \tilde{\psi}_d = 0, \quad \lim_{t\to\infty} \tilde{\psi}_q = 0. \tag{7}$$

III. Theoretical Comparison of the Indirect Field-Oriented Controllers

First, in this section, the S-IFO control algorithm for IM drives [3] is reinterpreted in terms of nonlinear control theory, in order to show the structural and stability properties of the equivalent error dynamics generated by this kind of controller. Second, the above and the I-IFO [16] controllers are compared in terms of their theoretical dynamic performance and robustness properties.

The general structure of an indirect field-oriented controller can be presented as

$$\mathbf{u} = \sigma\left[\begin{pmatrix} v_d \\ v_q \end{pmatrix} + \omega_0\mathbf{J}\mathbf{i}\right] \tag{8}$$

$$\dot{\varepsilon}_0 = \omega_0 = \omega + \alpha L_m \frac{i_q}{\psi^*} - \frac{v}{\psi^*}. \tag{9}$$

Substituting (8) and (9) into (1) the following field oriented decomposition results

$$\begin{aligned}\dot{\omega} &= \mu\left(\psi_d i_q - \tilde{\psi}_q i_d\right) - \frac{1}{J}T_L \\ \dot{i}_q &= -\gamma i_q + \alpha\beta\tilde{\psi}_q - \beta\omega\psi_d + v_q, \end{aligned} \tag{10}$$

$$\begin{aligned}\dot{\psi}_d &= -\alpha\psi_d + \omega_2\tilde{\psi}_q + \alpha L_m i_d \\ \dot{\tilde{\psi}}_q &= -\alpha\tilde{\psi}_q - \omega_2\tilde{\psi}_d + v \\ \dot{i}_d &= -\gamma i_d + \alpha\beta\psi_d + \beta\omega\tilde{\psi}_q + v_d \end{aligned} \tag{11}$$

where $\omega_2 = \omega_0 - \omega$ is the slip angular frequency.

According to (10) and (11), the field oriented transformation (9) and control algorithm (8), with compensation of the cross-coupling terms, decompose the original IM model into feedback connection of the two: electromechanical and electromagnetic subsystems, whose dynamics are given by (10) and (11), respectively. The flux modulus is the output of the electromagnetic subsystem (11), while the rotor speed is the output of the electromechanical subsystem (10). The two control inputs (v_d, v_q) can be selected to achieve the desired control objectives.

A. Standard Indirect Field-Oriented (S-IFO) Controller

Following the design procedure for cascaded systems, i_d^* and i_q^* are defined as references for currents i_d and i_q, respectively and the current regulation errors are given by

$$\tilde{i}_d = i_d - i_d^*, \qquad \tilde{i}_q = i_q - i_q^*. \tag{12}$$

Additionally, the following estimation errors are defined:

— for load torque (constant by assumption)

$$\tilde{T}_L = \frac{T_L}{J} - \hat{T}_L \tag{13}$$

where $\hat{T}_L$ is the integral part of the speed controller as it will be specified later;

— for current loops perturbation

$$\begin{aligned} \tilde{x}_d &= x_d - \frac{R_s}{\sigma}\frac{\psi^*}{L_m}, \\ \tilde{x}_q &= x_q - \left(\frac{\gamma}{\mu\psi^*}T_L + \beta\omega^*\psi^*\right) \end{aligned} \tag{14}$$

where x_d and x_q are the integral part of the current controllers as it will be defined later.

Note that, if the references of speed and flux are constant then perturbation defined in (14) are constant.

The equation for S-IFO controller can be mapped in the general controller structure (8) and (9). In particular in (9) v is imposed equal to zero and the expression of the voltage vector is derived from the following equations:

— flux modulus control algorithm

$$i_d^* = \frac{1}{\alpha L_m}\left(\alpha\psi^* + \dot{\psi}^*\right); \tag{15}$$

— proportional-integral (PI) speed controller

$$\begin{aligned} i_q^* &= \frac{1}{\mu\psi^*}\left(-k_\omega\tilde{\omega} + \hat{T}_L\right) \\ \dot{\hat{T}}_L &= -\dot{\tilde{T}}_L = -k_{\omega i}\tilde{\omega} \end{aligned} \tag{16}$$

where $k_\omega, k_{\omega i} > 0$ are the proportional and integral gains of the speed controller;

— PI current controllers

$$\begin{aligned} v_d &= -k_{id}\tilde{i}_d + x_d \\ \dot{x}_d &= -k_{ii}\tilde{i}_d \end{aligned} \tag{17}$$

$$\begin{aligned} v_q &= -k_{iq}\tilde{i}_q + x_q \\ \dot{x}_q &= -k_{ii}\tilde{i}_q \end{aligned} \tag{18}$$

where $k_{id}, k_{iq}, k_{ii} > 0$ are the current controllers proportional and integral gains.

Substituting (15)–(18) into (10) and (11), with $v = 0$, the final flux–speed error dynamics can be presented as (see Appendix A for detailed computation):

$$\begin{aligned} \dot{\tilde{\psi}}_d &= -\alpha\tilde{\psi}_d + \omega_2\tilde{\psi}_q + \alpha L_m\tilde{i}_d \\ \dot{\tilde{\psi}}_q &= -\alpha\tilde{\psi}_q - \omega_2\tilde{\psi}_d \\ \dot{\tilde{x}}_d &= -k_{ii}\tilde{i}_d \\ \dot{\tilde{i}}_d &= -(k_{id}+\gamma)\tilde{i}_d + \tilde{x}_d + \alpha\beta\tilde{\psi}_d + \beta\omega\tilde{\psi}_q \end{aligned} \tag{19}$$

$$\begin{aligned} \dot{\tilde{T}}_L &= k_{\omega i}\tilde{\omega} \\ \dot{\tilde{\omega}} &= -k_\omega\tilde{\omega} - \tilde{T}_L + \mu\psi^*\tilde{i}_q + \mu\left(\tilde{\psi}_d i_q - \tilde{\psi}_q i_d\right) \\ \dot{\tilde{x}}_q &= -k_{ii}\tilde{i}_q \\ \dot{\tilde{i}}_q &= -(k_{iq}+\gamma-k_\omega)\tilde{i}_q + \tilde{x}_q \\ &\quad - \left[\beta\psi^* + \frac{1}{\mu\psi^*}\left(k_\omega^2 - \gamma k_\omega - k_{\omega i}\right)\right]\tilde{\omega} \\ &\quad + \frac{1}{\mu\psi^*}(\gamma - k_\omega)\tilde{T}_L + \left(\frac{k_\omega}{\psi^*}i_q - \beta\omega\right)\tilde{\psi}_d \\ &\quad + \left(\alpha\beta - \frac{k_\omega}{\psi^*}i_d\right)\tilde{\psi}_q. \end{aligned} \tag{20}$$

According to (19) and (20) the S-IFO controller given by (8) and (9) with $v = 0$, and (15)–(18), decompose the IM model (1) into two interconnected systems: electromagnetic and electromechanical, whose error dynamics are given by (19) and (20) respectively. Asymptotic stability of the electromagnetic system can be established applying standard Lyapunov arguments and the Barbalat's Lemma (see Appendix B and [10] for similar systems). Hence the following result holds:

$$\lim_{t\to\infty}\left(\tilde{\psi}_d,\, \tilde{\psi}_q,\, \tilde{x}_d,\, \tilde{i}_d\right) = 0. \tag{21}$$

The error dynamics of the electromechanical (speed) subsystem (20) includes nominal [i.e., $(\tilde{\psi}_d,\, \tilde{\psi}_q)^T = 0$] linear time-invariant dynamics (with $\psi^* = \text{const.}$), which can always be designed to be asymptotically stable by the selection of current and speed controllers gains. In industrial vector controlled IM drives parameters $(k_\omega,\, k_{\omega i})$ and $(k_{iq},\, k_{ii})$ of speed and current PI controllers are designed, using the standard strategy usually adopted in cascaded DC drives, in order to guarantee time-scale separation between speed and current dynamics [2]. Well known "symmetrical optimum" can be used for evaluation of the gains of speed and current controllers.

According to nonlinear control theory the two feedback interconnected dynamics—flux subsystem (19) and speed subsystem (20)—are at least locally asymptotically stable, since the two interconnected systems have the following properties.

1) The nominal speed dynamics is linear and asymptotically stable.
2) The flux subsystem (19) is asymptotically stable for bounded speed trajectories.
3) The interconnection between the two subsystems is bilinear in the electromagnetic part and linear–bilinear in the electromechanical one.

From condition (21) and local asymptotic stability of the overall system error dynamics it follows that the standard flux–speed vector control algorithm ensures asymptotic flux modulus regulation together with asymptotic field orientation and asymptotic speed regulation under condition of constant load torque.

If the tuning parameters of the current and speed controllers are selected according to standard procedure for multi-loop cascaded systems, the overall error dynamics exhibits multi-time scale properties, i.e.:

1) the current error dynamics [last two equations in (19) and (20)] is the fastest one;

2) the speed error dynamics [first two equations in (20)] is at least few times slower;
3) the flux error dynamics [first two equations in (19)] is mainly defined by the rotor time constant $1/\alpha$ and it is the slowest one.

If the current controllers gains are increased, then the solution of full order dynamics will move to the reduced order one (current fed) given by (19) and (20) with $\tilde{i}_d \equiv \tilde{i}_q \equiv 0$, which is globally exponentially stable [16].

B. Improved Indirect Field-Oriented (I-IFO) Controller

In this subsection it is analyzed an improved indirect field-oriented (I-IFO) control algorithm for IM, which provides speed–flux tracking capabilities and reduced sensitivity to rotor parameters variations, while preserving all the advantages of the standard solution. The detailed development of the I-IFO algorithm is presented in [16]. Let us consider first the modified control algorithm of the flux subsystem

Flux vector controller

$$\dot{\varepsilon}_0 = \omega_0 = \omega + \alpha L_m \frac{i_q}{\psi^*} + \frac{\lambda}{\psi^*}\beta\omega\tilde{i}_d, \qquad \lambda > 0$$
$$i_d^* = \frac{1}{\alpha L_m}\left(\alpha\psi^* + \dot{\psi}^*\right). \tag{22}$$

Flux subsystem current controller

$$u_d = \sigma\left[-k_{id}\tilde{i}_d + \gamma i_d^* - \omega_0 i_q - \alpha\beta\psi^* + \frac{1}{\alpha L_m}\left(\alpha\dot{\psi}^* + \ddot{\psi}^*\right)\right]. \tag{23}$$

Substituting (22) and (23) into the second, third, and fourth equations of the IM model (1), the error dynamics of the flux subsystem becomes

$$\begin{aligned}\dot{\tilde{\psi}}_d &= -\alpha\tilde{\psi}_d + \omega_2\tilde{\psi}_q + \alpha L_M\tilde{i}_d\\ \dot{\tilde{\psi}}_q &= -\alpha\tilde{\psi}_q - \omega_2\tilde{\psi}_d - \lambda\beta\omega\tilde{i}_d\\ \dot{\tilde{i}}_d &= -(k_{id}+\gamma)\tilde{i}_d + \beta\left(\alpha\tilde{\psi}_d + \omega\tilde{\psi}_q\right).\end{aligned} \tag{24}$$

The equilibrium point $(\tilde{\psi}_d, \tilde{\psi}_q, \tilde{i}_d)^T = 0$ of the solutions of (24) is globally exponentially stable if the current controller proportional gain satisfies the following condition

$$k_{id} + \gamma > \frac{\alpha(\lambda\beta + L_m)^2}{4\lambda}. \tag{25}$$

The modified control algorithm of the electromechanical subsystem is

Speed controller

$$\begin{aligned}i_q^* &= \frac{1}{\mu\psi^*}\left(-k_\omega\tilde{\omega} + \hat{T}_L + \dot{\omega}^*\right)\\ \dot{\hat{T}}_L &= -k_{\omega i}\tilde{\omega}.\end{aligned} \tag{26}$$

Speed subsystem modified current controller

$$\begin{aligned}u_q &= \sigma\left[-k_{iq}\tilde{i}_q + \gamma i_q^* + \omega_0 i_d + \beta\omega\psi^* + \dot{i}_{q1}^* - \frac{1}{\psi^*}\left(\dot{\psi}^*\tilde{i}_q + \zeta\right)\right]\\ \dot{\zeta} &= k_{\eta i}\left(\psi^*\tilde{i}_q\right)\\ \dot{i}_{q1}^* &= \frac{1}{\mu\psi^*}\left[-k_\omega\left(-k_\omega\omega + \mu\psi^*\tilde{i}_q\right) + \dot{\hat{T}}_L + \ddot{\omega}^*\right] - \frac{\dot{\psi}^*}{\psi^*}i_q^*\end{aligned} \tag{27}$$

where $k_{\eta i} > 0$ is the integral gain of the modified current controller.

The speed error dynamics generated by the control algorithm (26) and (27) is given by

$$\begin{aligned}\dot{\tilde{T}}_L &= k_{\omega i}\tilde{\omega}\\ \dot{\tilde{\omega}} &= -k_\omega\tilde{\omega} - \tilde{T}_L + \mu\eta + \mu\left(\tilde{\psi}_d i_q^* - \tilde{\psi}_q i_d^*\right) + \frac{\mu}{\psi^*}\tilde{\psi}_d\eta - \mu\tilde{\psi}_q\tilde{i}_d\\ \dot{\zeta} &= k_{\eta i}\eta\\ \dot{\eta} &= -k_\eta\eta - \zeta - \frac{k_\omega}{\mu}\tilde{T}_L + \alpha\beta\psi^*\tilde{\psi}_q - \beta(\omega^* + \tilde{\omega})\psi^*\tilde{\psi}_d + \frac{k_\omega}{\mu}\left[\mu\left(\tilde{\psi}_d i_q^* - \tilde{\psi}_q i_d^*\right) + \frac{\mu}{\psi^*}\tilde{\psi}_d\eta - \mu\tilde{\psi}_q\tilde{i}_d\right]\end{aligned} \tag{28}$$

where $\eta = \psi^*\tilde{i}_q$, $k_{\eta i} > 0$, $k_\eta = (k_{iq} + \gamma) > 0$.

According to equations (24) and (28), the field-oriented controller (22), (23), (26), and (27) defines two coupled subsystems: a) the electromagnetic subsystem [d-subsystem with error state vector $\mathbf{x}_2 = (\tilde{\psi}_d, \tilde{\psi}_q, \tilde{i}_d)^T$]; b) the electromechanical subsystem [q-subsystem with error state vector $\mathbf{x}_1 = (\tilde{T}_L, \tilde{\omega}, \zeta, \eta)^T$].

In [16] it is shown that the equilibrium point $\mathbf{x} = (\mathbf{x}_1^T, \mathbf{x}_2^T)^T = 0$ of the system is globally exponentially stable and consequently control objectives (7) are satisfied. The nominal dynamics of the speed subsystem (28) ($\mathbf{x}_2 = \mathbf{0}$) is linear and IM parameters independent.

The block diagram of the two controllers is reported in Fig. 1. In order to emphasize the common origin, a single block diagram is reported. The light-shaded areas represent the added actions in the I-IFO controller, while the dark-shaded areas are integral actions present in the S-IFO controller only.

Comparing the error dynamics generated by the S-IFO controller (19) and (20) with that of the I-IFO controller (24) and (28), it can be concluded that they exhibit the following common structural properties.

1) The nominal [i.e., $(\tilde{\psi}_d, \tilde{\psi}_q) = \mathbf{0}$] speed subsystem dynamics is linear [for (20) only when $\psi^* = \text{const.}$] with the four parameters [proportional and integral gains of current (q-axis) and speed controllers] defining the closed loop dynamic performance.
2) Flux error subsystems (19) and (24) are asymptotically decoupled from speed dynamics and they are asymptotically stable [(19) only when $\psi^* = \text{const.}$ and for bounded trajectories of the speed subsystem variables].
3) The interconnection between the two subsystems has linear and bilinear properties.

Instead, the two error dynamics produced by the two controllers are different since.

1) The nominal speed subsystem dynamics (28) with $\mathbf{x}_2 = \mathbf{0}$, generated by the I-IFO controller, is linear for time varying flux reference and it is independent of motor parameters.
2) The flux subsystem dynamics (24) is globally exponentially stable, while system (19) has only semi-global asymptotic stability (requires selecting gain k_{id} according to the value of ω as reported in Appendix B).

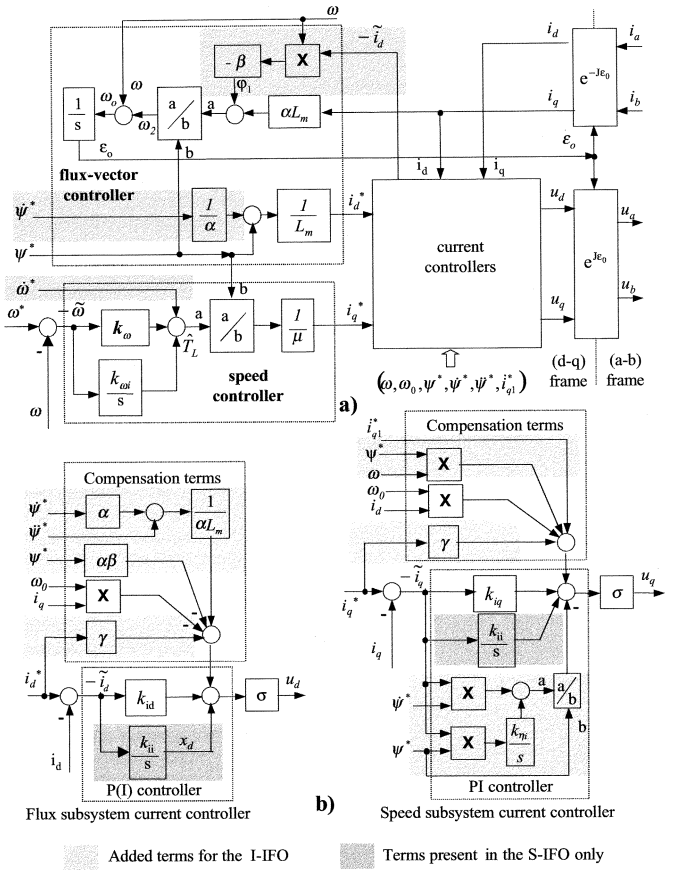


Fig. 1. Block diagram of IFO controllers: (a) speed and flux controllers and (b) current controllers.

3) The flux subsystem (19) is open loop, while (24) has negative feedback through the term $\lambda\beta\omega\tilde{i}_d$ (when $\omega \neq 0$). This yields an improved robustness with respect to rotor parameters variation, as it will enlighten in the following consideration.

Let consider the rotor time-constant perturbation for flux subsystems (19) and (24), given by $\alpha = \alpha_N + \Delta\alpha$. In both flux control algorithms (9) with $v \equiv 0$, (15), (17), (22), and (23) the nominal value α_N of the rotor time constant is used.

Under operation with constant flux reference ($\psi^* = \text{const.}$, $i_d^* = \psi^* L_m^{-1}$, $\dot{i}_d^* = 0$) and taking into account the time-scale separation between flux and i_d current dynamics (imposed by standard tuning procedure for cascaded systems) the reduced order solution for subsystem (19), obtained by using the singular perturbation theory [20], is characterized by $\dot{\tilde{i}}_d \equiv 0$ thanks to the integral action in current controller. In particular, it is

$$\begin{aligned}\dot{\tilde{\psi}}_d &= -\alpha\tilde{\psi}_d + \omega_2\tilde{\psi}_q \\ \dot{\tilde{\psi}}_q &= -\alpha\tilde{\psi}_q - \omega_2\tilde{\psi}_d + \Delta\alpha L_m i_q. \end{aligned} \tag{29}$$

From (29) it follows that the robustness properties in the case of S-IFO control are defined only by the value of α, i.e., they depend only on the natural features of the IM rotor circuit.

According to condition (25), flux subsystem (24) of I-IFO controller also exploits time-scale separation with a slow manifold for current error (obtained with $\dot{\tilde{i}}_d \equiv 0$) given by

$$\tilde{i}_d = (\gamma + k_{id})^{-1}\beta\left(\alpha\tilde{\psi}_d + \omega\tilde{\psi}_q\right). \tag{30}$$

Substituting (30) in the first two equation of (24), the slow flux dynamics is given by

$$\begin{aligned}\dot{\tilde{\psi}}_d =& -\alpha\left[1 - \beta L_m(\gamma + k_{id})^{-1}\right]\tilde{\psi}_d \\ &+ \left[\omega_2 + \alpha\beta L_m(\gamma + k_{id})^{-1}\omega\right]\tilde{\psi}_q \\ \dot{\tilde{\psi}}_q =& -\left[\alpha + \lambda\beta^2(\gamma + k_{id})^{-1}\omega^2\right]\tilde{\psi}_q \\ &- \left[\omega_2 + \alpha\lambda\beta^2(\gamma + k_{id})^{-1}\omega\right]\tilde{\psi}_d + \Delta\alpha L_m i_q. \end{aligned} \tag{31}$$

Equation (31) reflects the effect of negative feedback action delivering a proportional gain in q-axis flux equation augmented by a term equal to $\lambda\beta^2(\gamma + k_{id})^{-1}\omega^2$.

IV. Performance Specification and Experimental Results

A. Controllers Tuning

The error dynamics generated by the I-IFO controller (22), (23), (26) and (27) is given by (24) and (28). The tuning parameters of the flux subsystem are the proportional gain of the current controller k_{id} and the correction gain λ. The relationship between the two gains is given by condition (25).

The tuning parameters of the speed subsystem are the proportional gains k_ω, k_η and the integral gains $k_{\omega i}$, $k_{\eta i}$ of the speed and modified current controllers. According to the structure of the (28) the cascaded system structure allows for application of standard tuning relations

$$\frac{1}{\tau^2} = k_i \quad \text{and} \quad k_i = \left(\frac{k_p^2}{2}\right) \ (\delta = 0.707)$$

or

$$k_i = \left(\frac{k_p}{2}\right)^2 (\delta = 1) \tag{32}$$

where τ and δ are the time-constant and damping factor imposed for the second order error dynamics [see (28)], and k_i, k_p are the proportional and integral gains in each loop. The time scale separation is practically achieved with $\tau_s \geq (2 \text{ to } 4)\tau_i$ where indexes "s" and "i" stand for speed and current loops.

Both control algorithms presented in Section III were experimentally tested under the same controller's parameters tuning for two induction motors with the rated torque equal to 2.5 Nm and 6 Nm, respectively. The experimental tests for first IM has been carried out at the Laboratory of Electromechanics, National Technical University of Ukraine, and the second drive system has been tested at the Laboratory of Automation and Robotics of the University of Bologna. The operating conditions for the tests of 2.5 Nm IM are described below.

B. Operating Sequences

The operating sequences, reported in Fig. 2, are the following:

1) the machine is excited during the initial time interval $0 \div 0.25$ s using a flux reference trajectory starting at $\psi^*(0) = 0.02$ Wb and reaching the motor rated value of 0.9 Wb with the first and second derivatives equal to 3.5 Wb/s and 350 Wb/s^2 correspondingly;
2) the unloaded motor is required to track the speed reference trajectory, starting at $t = 0.6$ s from zero initial value and reaching the rated speed of 50 rad/s with the first and second derivatives equal to 700 rad/s^2 and 24 000 rad/s^3;

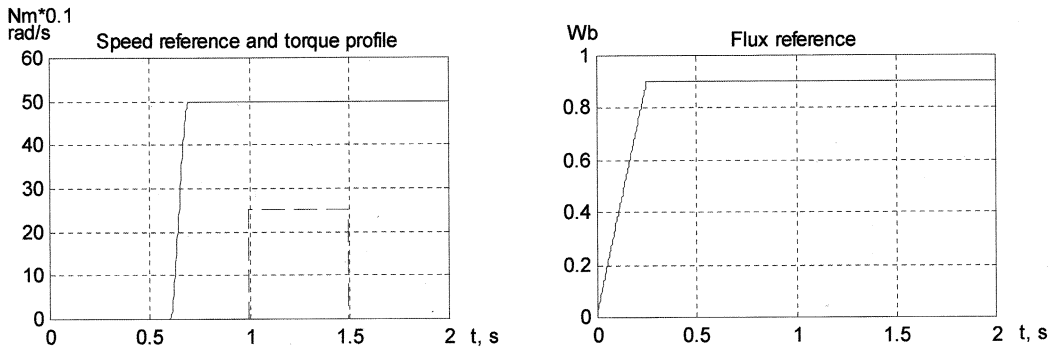


Fig. 2. Speed, flux references, and load torque profile.

3) at time $t = 1$ s a constant load torque, equal to the 120% of the motor rated value, is applied; at time $t = 1.5$ s load torque is set to zero.

C. Controllers Parameters

The controller's parameters, selected according to (32) were set at

$$k_\omega = 150, \quad k_{\omega i} = 11\,250, \quad k_{id} = k_{iq} = 700,$$
$$k_{ii} = k_{\eta i} = 122\,000, \quad \lambda\beta = 3.5.$$

D. Reference Trajectories

Tracking of the speed reference trajectory adopted requires a dynamic torque that is equal to the rated value of the motor. Flux and speed reference trajectories are presented in Fig. 2 using solid lines; dashed line in the same figure represents the load torque profile.

E. Experimental Set-Up

The experimental tests were carried out using a rapid prototyping station (RPS) developed at the Laboratory of Robotics and Automation, University of Bologna [21]. The RPS includes:

1) a Personal Computer acting as the Operator Interface for programming, debugging, program downloading, virtual oscilloscope function during the experiments;
2) a custom floating-point digital signal processor (DSP) board (based on TMS320C32) directly connected to the PC bus. The DSP board performs data acquisition (eight 12-bit A/D channels plus two interfaces for incremental encoder), implements control algorithms with programmable real-time tracing of selected variables, generates the PWM signals (two symmetrical three-phase PWM modulators with programmable dead time);
3) a 20-A/380 V_{RMS} three-phase inverter, operated at 10 kHz switching frequency during experiments;
4) a 2-pole, 50 Hz, 750 W induction servomotor, whose data are listed in the Appendix C;
5) a current controlled dc motor used to provide the load torque.

F. Measurement System and Controllers Implementation

In order to filter out the modulation ripple, the two stator phase currents, measured by Hall-effect zero-field sensors, are simultaneously and synchronously sampled at the symmetry point of the PWM signals. The motor speed is measured by means of a 1000 pulse/revolution incremental encoder. The sampling time for both standard and I-IFO controllers is set to 200 μs. In order to get the discrete time version of control algorithms the simple Euler method is used. Dead-time (1.5 μs) compensation is performed to achieve a better accuracy for the inverter output voltage.

G. Experimental Results

A first set of experiments, reported in Figs. 3 and 4, was performed to compare the dynamic performances of the two algorithms. The experimental results presented in Fig. 3 report the dynamic performance of the S-IFO controller during speed trajectory tracking. The transient performance is characterized by a maximum speed error of about 2 rad/s during reference trajectory tracking and about 4 rad/s during constant load torque rejection.

The experimental results presented in Fig. 4 demonstrate the dynamic performance of the I-IFO controller adopting the same tuning as for the S-IFO controller. Significant improvement of the speed tracking is reported. The speed tracking performance (maximum speed error of about 0.3 rad/s) is about one order better compared with that of the S-IFO controller. Besides, the I-IFO controller presents a significant overshoot reduction in the i_q current. The transient behavior of the S-IFO and I-IFO controllers during load compensation is the same.

A second set of experiments was made to compare the dynamic performance of the two controllers, when parameter $\hat{\alpha} = \hat{R}_r/\hat{L}_r$ (inverse of rotor time constant) used in control algorithm is different from actual one. Fig. 5(a) and (b) demonstrate the transients with the S-IFO control obtained for $\hat{\alpha} = 10$ 1/s ($1.7\alpha_N$) and $\hat{\alpha} = 2.9$ 1/s ($0.5\alpha_N$). During these tests load torque (120% of rated value) is applied at time $t = 1$ s and remains constant during time interval of experiment. As it is shown in Fig. 5(a) the significant degradation of the transient performance occurs for parameter $\hat{\alpha}$ higher then rated value. The steady state value of i_q axis current is almost 60% larger than the nominal regime. On contrary, no relevant difference is observed for $\hat{\alpha} = 2.9$ 1/s [Fig 5(b)] as compared with the rated transient. Only slightly higher torque current is required to produce the same motor torque. As it is discussed in [11], $\hat{\alpha} > \alpha_N$ produces a reduction of the rotor flux impairing transient performances and increasing the torque current. Differently, when

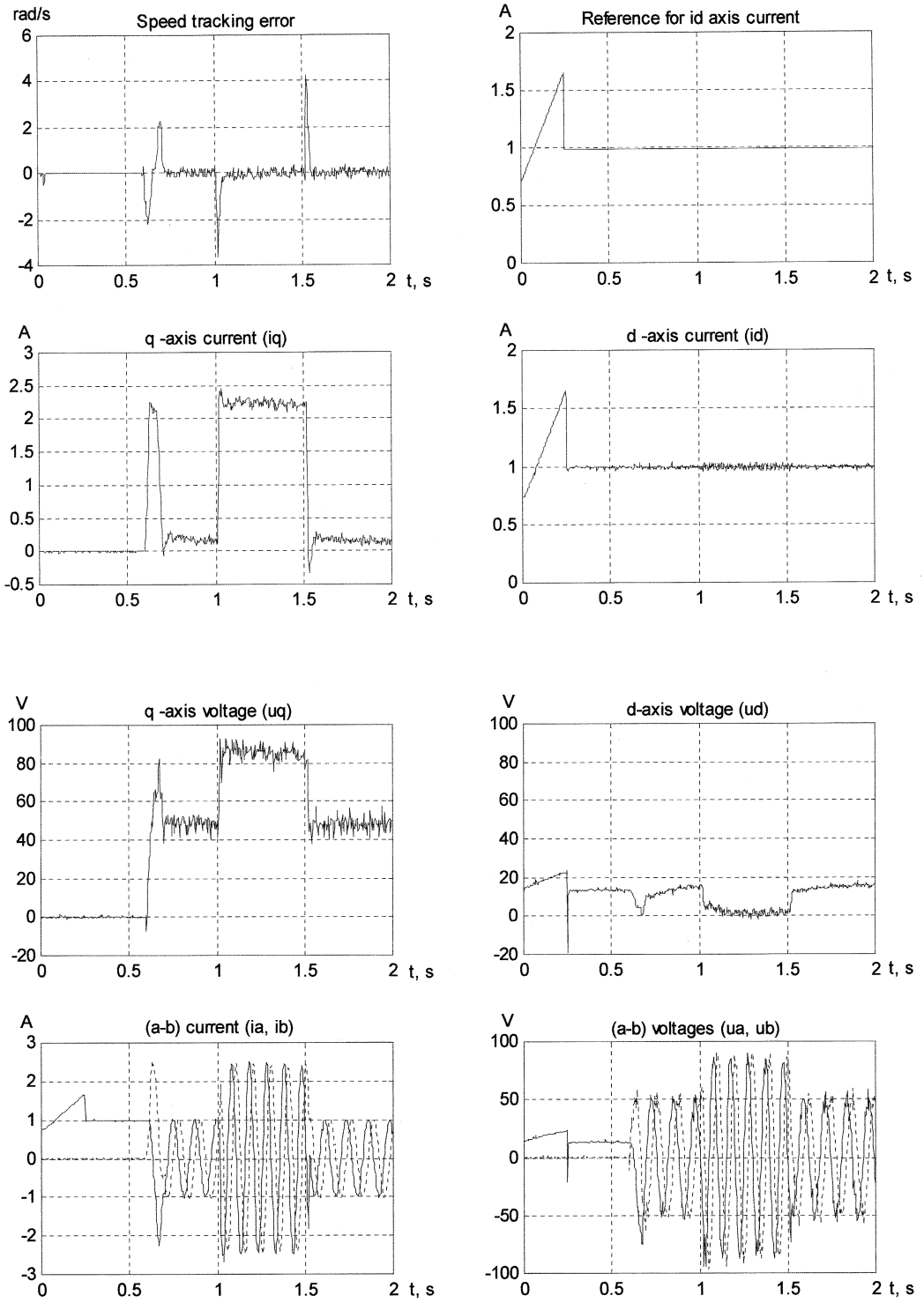


Fig. 3. Dynamic behavior of the S-IFO controller with $\hat{\alpha}$ equal to the nominal one.

$\hat{\alpha} < \alpha_N$, the motor electromagnetic system enters into saturation region, causing some increasing of the stator current modulus. In fact, owing to the magnetic saturation, the IM operates with almost constant flux modulus, but with wrong field orientation.

The results of the same test for I-IFO controller are reported in Fig. 6. Comparison of the transients, reported in Figs. 4 and 6, shows that improved indirect field-oriented controller demonstrates strong robustness properties with respect of rotor time constant variations. No significant difference can be noted in transients in nominal (Fig. 4) and perturbed (Fig. 6) conditions.

A third set of experiments was made to compare the system efficiency under steady-state condition of operation. The comparison was referred to steady state behavior of the two controllers for two different induction motors, whose rated data are listed in Appendix C. The first induction machine (2.5 Nm

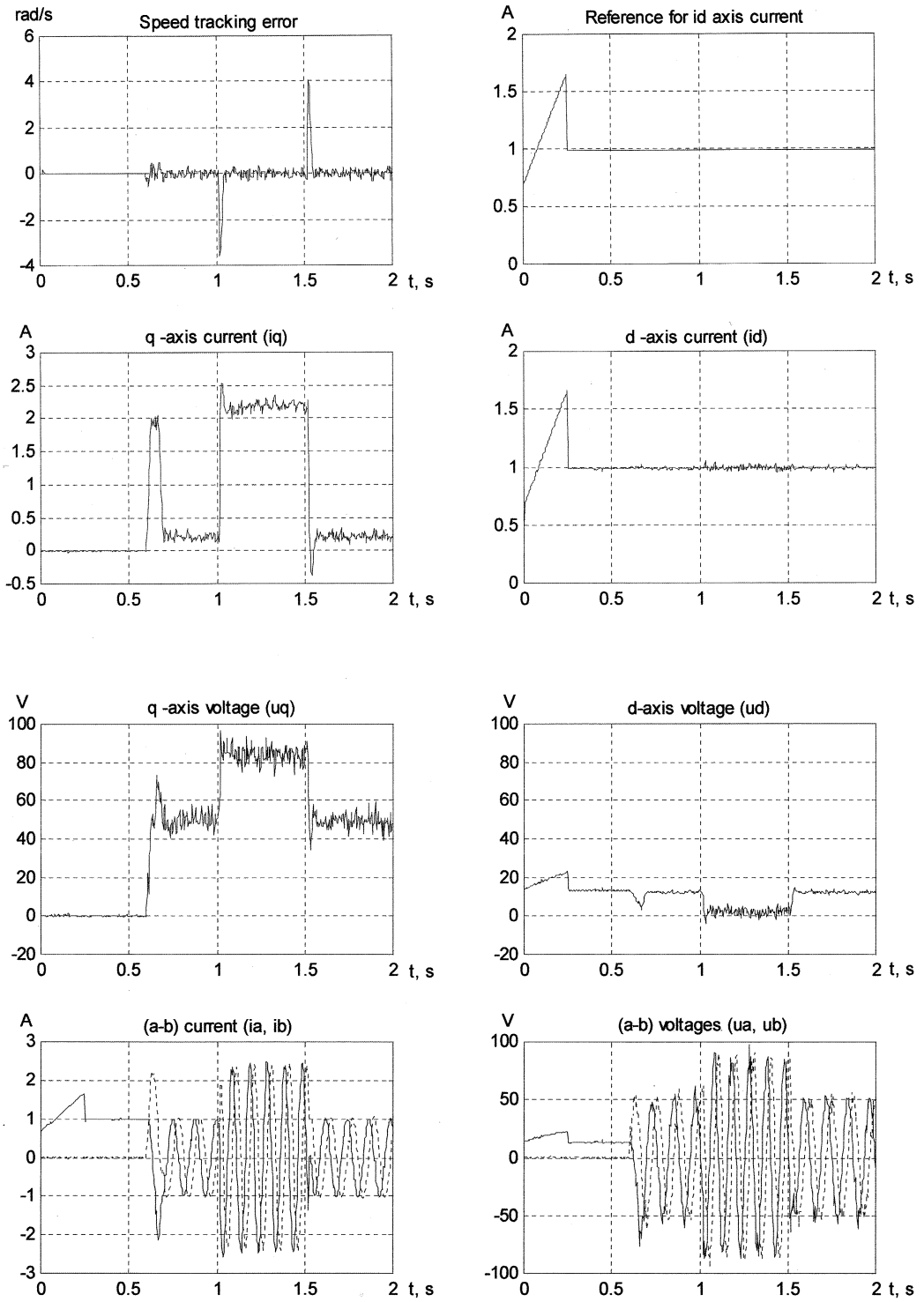


Fig. 4. Dynamic behavior of the I-IFO controller with $\hat{\alpha}$ equal to the nominal one.

rated torque), have been used for dynamic tests presented in this paper. The dynamical tests for second IM (6 Nm rated torque, whose rated data are given in Appendix C in bracket) have been performed as well but they are not shown. In fact, the dynamic performance obtained during speed trajectory tracking with dynamic torque equal to 350% of rated motor torque is quite closed to results previously obtained by authors for other much more complex speed–flux tracking controller, reported in [10]. Even if the control algorithm [10] is quite different from the one discussed here, the results are similar due to uniqueness of solutions for IM inverse dynamics, when ideal tracking is achieved. During investigation of steady state performance, a fixed reference speed of 50 rad/s (100 rad/s for second motor) is imposed. Different values of load torque are applied to verify how the i_q (torque current) varies when wrong values of the parameter $\hat{\alpha}$ are used in the two control algorithms. During the experiments

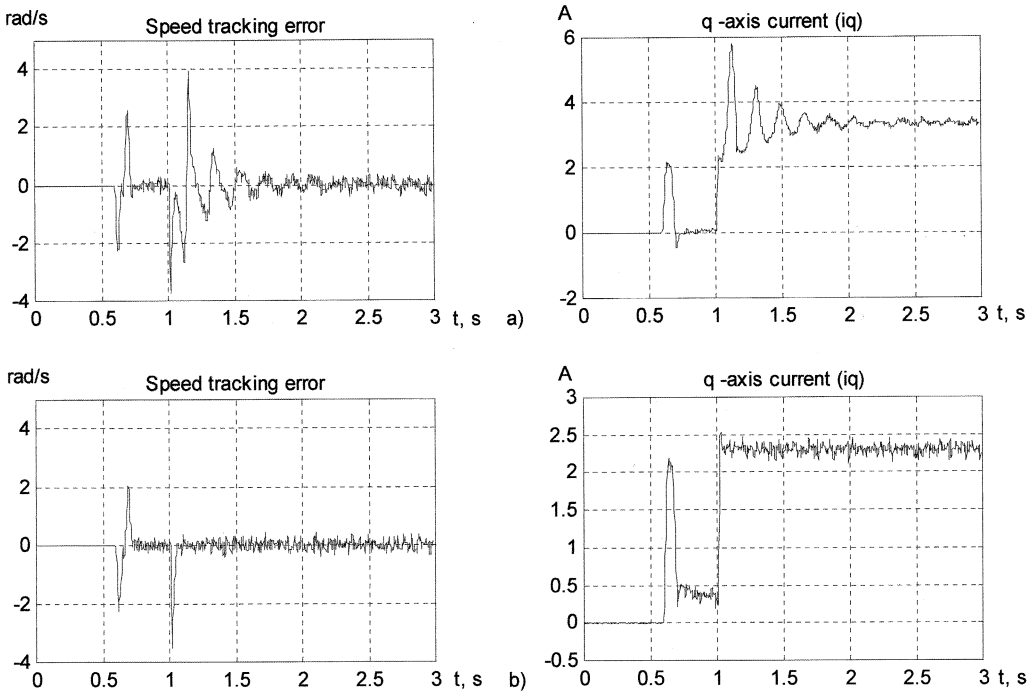


Fig. 5. Dynamic behavior of S-IFO controller with $\hat{\alpha}$ equal to (a) $1.7\alpha_N$ and (b) $0.5\alpha_N$.

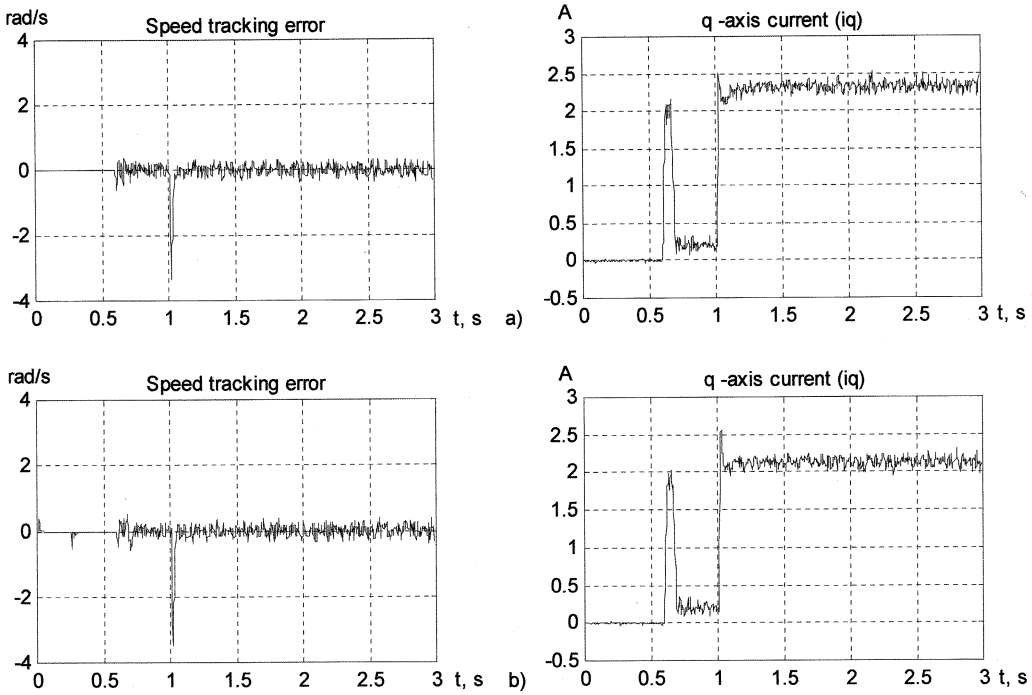


Fig. 6. Dynamic behavior of I-IFO controller with $\hat{\alpha}$ equal to (a) $1.7\alpha_N$ and (b) $0.5\alpha_N$.

the i_d (flux current) is set to rated value, in order to get the nominal rotor flux. The steady-state regulation errors $\tilde{\omega}$ and $\tilde{i}_d$ are negligible for both algorithms.

The experimental test with 2.5 Nm IM, whose results are reported in Fig. 7, are executed in the following way. Constant load torque equal to 120% of rated value has been imposed, fixing the output mechanical power on the level of 150 W. Different values of parameter $\hat{\alpha}$ are used in both control algorithms. For each value of $\hat{\alpha}$ the steady state i_q current and output inverter active power $P_a = (3/2)(u_a i_a + u_b i_b)$ have been recorded. In Fig. 7 the i_q current and active power P_a of the S-IFO controller are shown using dashed lines, while the same variables of the I-IFO controller are reported with continuous lines. The lower trace in Fig. 7(b) corresponds to mechanical output power of the IM.

The experimental results reported in Fig. 8 has been performed for 6 Nm IM using the same test procedure but for different values of the load torque. The controller parameters

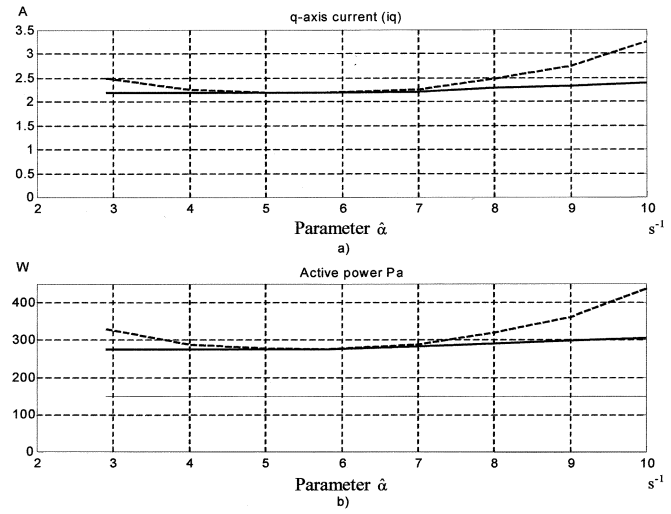


Fig. 7. Steady state characteristics of 2.5 Nm IM. (a) "Torque current," i_q, versus $\hat{\alpha}$ used in the control algorithms. (b) Active power, P_a, versus $\hat{\alpha}$ used in the control algorithms. Standard IFO controller: dashed lines; Improved IFO controller: continuous lines.

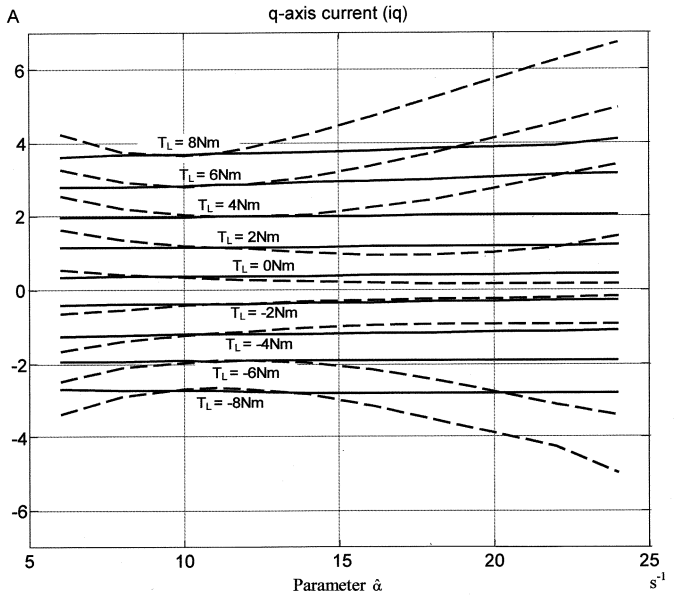


Fig. 8. Steady state characteristics of 6 Nm IM. "Torque current," i_q, versus $\hat{\alpha}$ used in the control algorithms. Standard IFO controller: dashed lines; Improved IFO controller: continuous lines.

during this test were set at $k_\omega = 375$, $k_{\omega i} = 7 * 10^4$, $k_{id} = k_{iq} = 1500$, $k_{ii} = k_{\eta i} = 5 * 10^5$, $\lambda = 0.2$. Positive values of T_L indicate a load torque opposite with respect to the rotation, while negative values represent loads in the same direction of the rotation. When the load torque is null, the motor torque is not null since viscous and static frictions are present.

The experimental results reported in Figs. 7 and 8 show that the I-IFO controller is able to keep almost a constant torque current even with large $\hat{\alpha}$-parameter error. The i_q current imposed by the S-IFO controller considerably increases when a wrong $\hat{\alpha}$ is used. This means that, as compared to the S-IFO controller, the I-IFO controller guarantees more robust stabilization of the rotor flux vector (both angular position and amplitude) under rotor time constant variations. As a result, in most of the operating condition, a reduced i_q current is required to compensate for a given load torque, thus considerably increasing the system overall energy efficiency. As it is reported in Fig. 7(b) the efficiency of the electromechanical energy conversion process degrades almost twice for S-IFO when $\hat{\alpha} = 1.7\alpha_N$, while I-IFO guarantees stabilization of the efficiency approximately on the rated level.

As reported in [22], during small loading conditions a reduction of flux level is required in order to keep maximum torque per Ampere ratio [22]. From Fig. 8, it can be noted that a similar effect occurs by chance for S-IFO controller (tuned with parameter $\hat{\alpha}$ grater than the actual motor value) due to wrong field orientation. For the I-IFO controller an energy efficient flux control strategy can be consciously applied while preserving the field orientation. Moreover, since the flux subsystem is asymptotically decoupled from the speed control, operation with time-varying flux level does not generate speed transients.

Experimental testing is well in agreement with the simulation results reported in [16]. Experiments confirm that the proposed I-IFO controller provides significant improvement of the dynamic performance during speed–flux tracking as well as improved energy efficiency as compared to standard solutions adopted in industrial drives.

V. Conclusion

In this paper, an improved indirect field-oriented (I-IFO) control algorithm with speed–flux tracking capability is compared with the standard (S-IFO) solutions adopted in industrial drives. It is theoretically and experimentally shown that the I-IFO solution can be viewed as an actual improvement of standard control schemes. It allows achieving higher dynamic performance and improved robustness with respect to rotor parameter variations, leading to improved energy efficiency. In addition, the I-IFO controller ensures asymptotic decoupling of the speed and flux subsystems as well as asymptotic linearization of the speed subsystem. Improvement of performance and robustness is achieved with a simple, theoretically proven, modification of the standard controller structure. Simple implementation, controller's parameter selection and practical tuning (conceptually the same adopted in standard cascaded industrial drives) make the I-IFO controller suitable for practical implementation.

Appendix A

Using the definitions (12) and (13) with conditions $\psi^* = \text{const.}$, $\omega^* = \text{const.}$, $v = 0$, equations and can be written as

$$\begin{aligned}
\dot{\tilde{\omega}} &= \mu\psi^* i_q^* + \mu\psi^* \tilde{i}_q - \hat{T}_L - \tilde{T}_L + \mu\left(\tilde{\psi}_d i_q - \tilde{\psi}_q i_d\right) \\
\dot{\tilde{i}}_q &= -\gamma\tilde{i}_q - \gamma i_q^* + \alpha\beta\tilde{\psi}_q - \beta\omega\tilde{\psi}_d - \beta\tilde{\omega}\psi^* \\
&\quad - \beta\omega^*\psi^* + v_q - \dot{i}_q^* \qquad \text{(A1)} \\
\dot{\tilde{\psi}}_d &= -\alpha\tilde{\psi}_d + \omega_2\tilde{\psi}_q + \alpha L_m\tilde{i}_d + \alpha L_m i_d^* - \alpha\psi^* - \dot{\psi}^* \\
\dot{\tilde{\psi}}_q &= -\alpha\tilde{\psi}_q - \omega_2\tilde{\psi}_d \\
\dot{\tilde{i}}_d &= -\gamma\tilde{i}_d - \left(\frac{R_s}{\sigma} + \alpha L_m\beta\right)\frac{1}{L_m}\psi^* \\
&\quad + \alpha\beta\left(\psi^* + \tilde{\psi}_d\right) + \beta\omega\tilde{\psi}_q + v_d - \dot{i}_d^*. \qquad \text{(A2)}
\end{aligned}$$

Substituting control algorithm (15)–(18) in (A1) and (A2) with

$$\dot{i}_{q1}^{*} = \frac{1}{\mu\psi^{*}}\left\{-k_{\omega}\left[-k_{\omega}\tilde{\omega} - \tilde{T}_L + \mu\psi^{*}\tilde{i}_q + \mu\left(\tilde{\psi}_d i_q - \tilde{\psi}_q i_d\right)\right] + \dot{\hat{T}}_L\right\} \quad \text{(A3)}$$

computed using (16) and tacking into account definition (14), the resulting error dynamics is given by (19) and (20).

Appendix B

Let consider the following Lyapunov function for subsystem (19)

$$V = \tfrac{1}{2}\left(\tilde{\psi}_d^2 + \tilde{\psi}_q^2 + \gamma_1\tilde{i}_d^2 + \gamma_2\tilde{x}_d^2\right) \qquad \gamma_1,\, \gamma_2 > 0 \quad \text{(B1)}$$

whose time derivative along the solutions of (19) is equal to

$$\dot{V} = -\left([\,\tilde{\psi}_d \quad \tilde{i}_d\,]\,\mathbf{Q_1}\begin{bmatrix}\tilde{\psi}_d\\ \tilde{i}_d\end{bmatrix} + [\,\tilde{\psi}_q \quad \tilde{i}_d\,]\,\mathbf{Q}_2\begin{bmatrix}\tilde{\psi}_q\\ \tilde{i}_d\end{bmatrix} + [\,\tilde{\psi}_q \quad \tilde{i}_d\,]\,\mathbf{Q}_3\begin{bmatrix}\tilde{\psi}_q\\ \tilde{i}_d\end{bmatrix}\right) \quad \text{(B2)}$$

where

$$\mathbf{Q_1} = \begin{bmatrix}\alpha & -\dfrac{(\alpha L_m + \gamma_1\alpha\beta)}{2}\\ -\dfrac{(\alpha L_m + \gamma_1\alpha\beta)}{2} & \gamma_1(k_{id1} + \gamma)\end{bmatrix},$$

$$\mathbf{Q_2} = \begin{bmatrix}\dfrac{\alpha}{2} & -\dfrac{\gamma_1\omega^{*}\beta}{2}\\ -\dfrac{\gamma_1\omega^{*}\beta}{2} & \gamma_1 k_{id2}\end{bmatrix}$$

and

$$\mathbf{Q}_3 = \begin{bmatrix}\dfrac{\alpha}{2} & -\dfrac{\gamma_1\tilde{\omega}\beta}{2}\\ -\dfrac{\gamma_1\tilde{\omega}\beta}{2} & \gamma_1 k_{id3}\end{bmatrix},$$

with $\gamma_2 = k_{ii}^{-1}\gamma_1$ and $k_{id} = k_{id1} + k_{id2} + k_{id3}$. Note that the speed, ω, has been split in reference and error according to (6).

Assuming that a bounded reference, $|\omega^{*}| < w$, for any bounded speed error trajectory $|\tilde{\omega}(t)| < w_1$, it is possible to choose the gains k_{id1}, k_{id2}, k_{id3} large enough to guarantee

$$\begin{aligned} 4\alpha\gamma_1(k_{id1} + \gamma) &> (\alpha L_m + \gamma_1\alpha\beta)^2,\\ 4\alpha\gamma_1 k_{id2} &> (\gamma_1 w\beta)^2,\\ 4\alpha\gamma_1 k_{id3} &> (\gamma_1 w_1\beta)^2 \end{aligned} \quad \text{(B3)}$$

hence the matrixes $\mathbf{Q_1}$, $\mathbf{Q_2}$ and $\mathbf{Q_3}$, are all positive definite and

$$\dot{V} \le 0. \quad \text{(B4)}$$

Note that the larger is k_{id3}, the larger can be the bound w_1 for the speed error.

From (B4) it follows that:

- $V(t)$ is a lower bounded nonincreasing function, hence it has finite limit as $t \to \infty$;
- the state vector of (19) is globally stable in the sense of Lagrange, then the state trajectories are bounded for every bounded initial condition; hence the $\ddot{V}(t)$ is bounded and the $\dot{V}(t)$ is uniformly continuous;

Therefore, applying the Barbalat's Lemma, it results

$$\dot{V} \xrightarrow{t\to\infty} 0. \quad \text{(B5)}$$

This implies

$$[\,\tilde{\psi}_d \quad \tilde{\psi}_q \quad \tilde{i}_d\,]^T \xrightarrow{t\to\infty} \mathbf{0}. \quad \text{(B6)}$$

From this result, applying again the Barbalat's Lemma to $\tilde{i}_d$, $\dot{\tilde{i}}_d$ (adding the technical hypothesis of $\dot{\tilde{\omega}}$ bounded), the following result holds:

$$\tilde{x}_d \xrightarrow{t\to\infty} 0. \quad \text{(B7)}$$

Appendix C

Nominal parameters of the Induction Motors adopted for the experimental test

Induction motor data:

Rated power	$750\ (900)$ W
Rated torque	$2.5\ (6, 0)$ Nm
Number of poles	$2\ (4)$
Excitation current	$1\ (2.05)$ A
Rated current	$2.4\ (3.4)$ A
Stator resistance	$R_s = 11\ (6.6)\ \Omega$
Rotor resistance	$R_r = 5.6\ (5.3)\ \Omega$
Magnetization inductance	$L_m = 0.91\ (0.45)$ H
Stator inductance	$L_s = 0.95\ (0.475)$ H
Rotor inductance	$L_r = 0.95\ (0.47)$ H
Total inertia	$J = 0.005\ (0.01)$ kgm^2.

References

[1] F. Blaschke, "The principle of field orientation applied to the new transvector closed-loop control system for rotating field machines," *Siemens-Rev.*, vol. 39, pp. 217–220, 1972.

[2] W. Leonhard, *Control of Electric Drives*. Berlin, Germany: Springer-Verlag, 1995.

[3] D. W. Novotny and T. A. Lipo, *Vector Control and Dynamics of AC Drives*. Oxford, U.K.: Clarendon, 1996.

[4] G. C. Verghese and S. R. Sanders, "Observer for flux estimation in induction machines," *IEEE Trans. Ind. Electron.*, vol. 35, pp. 85–94, Feb. 1988.

[5] P. L. Jansen and R. D. Lorenz, "A physically insightful approach to the design and accuracy assessment of flux observers for field-oriented induction machine drives," *IEEE Trans. Ind. Applicat.*, vol. 30, pp. 101–110, Jan./Feb. 1994.

[6] L. Harnefors, "Design and analysis of general rotor–flux-oriented vector control systems," *IEEE Trans. Ind. Electron.*, vol. 48, pp. 383–390, Apr. 2001.

[7] K. Hasse, "Zum dynamischen verhalten der asynchron maschine bei betrieb mit variabler stander-frequenz und standerspannung," in *Proc. Electrotech. Zeitung ETZ—A89 Conf.*, 1968, pp. 77–81.

[8] R. Ortega and D. Taoutaou, "Indirect field-oriented speed regulation for induction motors is globally stable," *IEEE Trans. Ind. Electron.*, vol. 43, pp. 340–341, Apr. 1996.

[9] P. J. Nicklasson, R. Ortega, and G. Espinosa, "Passivity-based control of a class of Blondell–Park transformable electric machines," *IEEE Trans. Automat. Contr.*, vol. 42, pp. 629–647, May 1997.

[10] S. Peresada, A. Tonielli, and R. Morici, "High performance indirect field-oriented output-feedback control of induction motors," *Automatica*, vol. 35, pp. 1033–1047, 1999.

[11] R. Marino, S. Peresada, and P. Tomei, "Output feedback control of current-fed induction motors with unknown rotor resistance," *IEEE Trans. Contr. Syst. Technol.*, vol. 4, pp. 336–347, July 1996.

[12] X. Roboam, C. Andrieux, B. de Fornel, and J. C. Hapiot, "Rotor flux observation and control in squirrel-cage induction motor: Reliability with respect to parameters variations," *Proc. Inst. Elect. Eng. D.*, vol. 139, pp. 363–370, 1992.

[13] T. Matsuo and T. A. Lipo, "A rotor parameter identification scheme for vector controlled induction motor drives," *IEEE Trans. Ind. Applicat.*, vol. 21, pp. 624–632, May/June 1985.
[14] R. Marino, S. Peresada, and P. Tomei, "Global adaptive output feedback control of induction motors with uncertain rotor resistance," *IEEE Trans. Automat. Contr.*, vol. 44, pp. 967–983, May 1999.
[15] P. Vas, *Artificial-Intelligence-Based Electrical Machines and Drives*. Oxford, U.K.: Oxford Press, 1999.
[16] S. Peresada and A. Tonielli, "High performance robust speed–flux tracking controller for induction motor," *Int. J. Adaptive Contr. Signal Processing*, vol. 14, no. 2, pp. 177–200, 2000.
[17] D. M. Dawson, J. Hu, and T. C. Burg, *Nonlinear Control of Electric Machinery*. New York: Marcel Dekker, 1998.
[18] K. C. Kim, R. Ortega, A. Charara, and J. P. Vilain, "Theoretical and experimental comparison of two nonlinear controllers for current fed induction motors," *IEEE Trans. Contr. Syst. Technol.*, vol. 5, pp. 340–348, May 1997.
[19] C. Cecati and N. Rotondale, "Torque and speed regulation of induction motors using the passivity theory approach," *IEEE Trans. Ind. Electron.*, vol. 46, pp. 119–127, Feb. 1999.
[20] P. V. Kokotovic, H. K. Khalil, and J. O'Reilly, *Singular Perturbation Methods in Control: Analysis and Design*. New York: Academic, 1986.
[21] R. Morici, C. Rossi, and A. Tonielli, "Fast prototyping of nonlinear controllers for electric motors drives," in *Proc. IFAC'93, 12th World Congress*, Sydney, Australia, 1993.
[22] O. Wasynczuk, S. D. Sudhoff, K. A. Corzine, J. L. Tichenor, P. C. Krause, I. G. Hansen, and L. M. Taylor, "A maximum torque per Ampere control strategy for induction motor drives," *IEEE Trans. Energy Conv.*, vol. 13, pp. 163–169, June 1998.



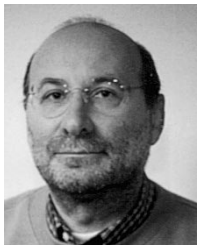
Sergei Peresada was born in Donetsk, Ukraine, on January 14, 1952. He received the M.S. degree in electrical engineering from Donetsk Polytechnical Institute, Ukraine, in 1974, and the Ph.D. degree in electrical engineering from the Kiev Polytechnical Institute, Kiev, Ukraine, in 1983.

From 1974 to 1977, he was a Research Engineer in the Department of Electrical Engineering, Donetsk Polytechnical Institute. Since 1977, he has been with the Department of Electrical Engineering, Kiev Polytechnical Institute, where he is currently a Professor. From 1985 to 1986, he was a Visiting Professor in the Department of Electrical and Computer Engineering, University of Illinois at Urbana, Champaign. His research interests include applications of modern control theory (nonlinear control, adaptation, VSS control) in electromechanical systems, model development, and control of electrical drives and internal combustion engines.



Andrea Tilli was born in Bologna, Italy, on April 4, 1971. He received the "Laurea" degree in electronic engineering and the Ph.D. degree in system science and engineering from the University of Bologna, Italy, in 1996 and 2000, respectively. His thesis was on nonlinear control of standard and special asynchronous electric machines.

Since 1997, he has been with the Department of Electronics, Computer and System Science (DEIS), University of Bologna, where, in July 2000, he won a research grant for the modeling and control of complex electromechanical systems. He became a Research Associate at DEIS in 2001. His current research interests include applied nonlinear control techniques, adaptive observers, variable structure systems, electric drives, automotive systems, active power filters, and DSP-based control architectures.



Alberto Tonielli (A'80) was born in Tossignano, Bologna, Italy, on April 1, 1949. He received the Dr.Ing. degree in electronic engineering from the University of Bologna, Italy, in 1974.

In 1975, he joined the Department of Electronics, Computer and System Science (DEIS), University of Bologna, with a grant from the Ministry of Public Instruction. In 1979, he started teaching as an Assistant Professor. In 1980, he became Permanent Researcher. In 1981, he spent two quarters at the University of Florida, Gainesville, as Visiting Associate Professor. In 1985, he became Associate Professor of Control System Technologies at the University of Bologna, where he is currently Professor of automatic control. His current research interests are in the fields of nonlinear and sliding mode control for electric machines, nonlinear observers, robotics, and DSP-based control architectures.

View publication stats